Biomass Conversion and Biorefinery (2024) 14:12283–12296
https://doi.org/10.1007/s13399-022-03272-9

ORIGINAL ARTICLE

Apricot seed shell: an agro-waste biosorbent for acid blue193 dye adsorption

A. Hashem[1] · Chukwunonso O. Aniagor[2] · Osama M. Morsy[1,3] · A. Abou-Okeil[1] · A. A. Aly[1]

Received: 7 June 2022 / Revised: 20 August 2022 / Accepted: 29 August 2022 / Published online: 17 September 2022
© The Author(s) 2022, corrected publication 2022

Abstract

Locally available apricot (*Prunus armeniaca* L.) seed shell wastes were utilized for the preparation of an efficient dye biosorbent. The as-prepared apricot seed shell powder (*ASP*) was thoroughly characterized using FTIR, SEM-EDX, XRD, BET surface area, and pH_{PZC} measurements to elucidate its functional groups, as well as its surface texture morphology and charge. The effect of several process variables (such as contact time, biosorbent dosage, pH, temperature, and initial concentration) on the dye uptake capacity was also investigated. Based on the experimental finding, the following optimum process conditions were established in the study: pH 2.0, 0.2 g/L adsorbent mass, 30 °C, and time of 120 min. The BET surface area, pore volume, and average pore size of the *ASP* were estimated as 97.493 m^2/g, 0.0691 cm^3/g, and 1.922 nm, respectively. The experimental equilibrium and kinetic data were properly described by the Temkin isotherm and pseudo-first-order kinetics model, respectively. Therefore, the effectiveness of *ASP* as an acid blue 193 dye biosorbent was established in the study.

Keywords Agro-waste · Kinetics · Isotherm · Thermodynamics · Acid dye

1 Introduction

Synthetic dyes are important raw materials of high demand in textile, paper and pulp, leather tanning, and food processing industries. According to Sen et al. [1], about 7×10^5 tones of different synthetic dyes are produced annually worldwide and the textile industry alone consumes more than 10,000 tons/year. Consequently, 1.0% of this total consumption by textile industries ends up as pollutants in the hydrosphere [2]. Asides from the textile industry, other process industries also contribute a substantive volume of dye contaminants into the aquatic environment, although the exact discharge data are unknown. These dye pollutants generally impart undesirable colouration which limits the penetration of sunlight to the water body and further constitutes photochemical/biological incursion into the aquatic ecosystem [3]. Hence, their continued presence in the aquatic environment constitutes serious concern to environmental scientists and demands attention.

In an attempt to address the issues of dye contamination, photocatalytic decomposition [4], chemical oxidation [5–7], and biological degradation [8] techniques have been studied with some noticeable limitations. For instance, due to dye's resistance to oxidizing agents and aerobic digestion, the chemical oxidation and biological degradation techniques are respectively less efficient [9]. Similarly, photocatalytic decomposition is bedeviled by high operational costs coupled with the difficulty of separating the dispersed photocatalysts after the treated stream [10]. However, the adsorption technique is considered a viable treatment option due to its process efficiency, design flexibility, and cost-effectiveness (due to the ready availability of agro-waste adsorbent precursors) [11–13]. Asides from their cheap availability, these agro-wastes consist mainly of cellulose, hemicelluloses, and lignin which provide relevant functional groups (such as hydroxyl, carboxyl, phenols, and methoxy) which are necessary for efficient dye uptake [14, 15]. A wide range of agricultural waste materials such as canola hullwood, sawdust,

✉ A. Hashem
alihashem2000@yahoo.com

✉ Chukwunonso O. Aniagor
co.aniagor@unizik.edu.ng

[1] Textile Research Division, National Research Center, Dokki, Cairo, Egypt

[2] Department of Chemical Engineering, Nnamdi Azikiwe University, P.M.B. 5025, Awka, Nigeria

[3] Arab Academy for Science, Technology & Maritime Transport, Arab League, Cairo 2033, Egypt

peat, and coconut shells have been used in their natural form for adsorbing dye pollutants [16–18].

Apricot, *Prunus armeniaca* L., is a member of the Rosaceae plant family which is widely cultivated in North Africa, Asia, and Europe [19]. Notably, 60% of the global apricot fruit production originates from the countries in the Mediterranean basin. With an average production of 16,333.5 tons per hectare, Egypt has the highest apricot harvest ratio [20]. Consequently, the huge volume of apricot shells generated during fruit and seed processing is either discarded as agricultural wastes, used as a raw material for activated carbon production [21], as small scale energy source [22], or as an organic additive for improving soil fertility [23]. To further enhance its environmental usefulness, this agro-waste is applied as a low-cost dye adsorbent. The efficient adsorptions of Astrazone Black, textile dye Levafix Blue CA, and leather dye Brown VBR have been reported [24, 25]. Similarly, activated carbon adsorbents produced from apricot seed shells have been applied by Ammar et al. [26] and adhami et al. [27] for the adsorption of methylene blue dye. So far, the literature survey showed that unmodified apricot shells were exclusively applied for heavy metal biosorption [23, 28]. The use of apricot seed shell (*ASP*) as an adsorbent for the removal of anionic dyes has never been mentioned before in literature. Furthermore, the effects of different process variables on the dye uptake, adsorbents' instrumental characteristics, adsorption modeling (kinetic and isotherm studies), and thermodynamics investigation were elucidated.

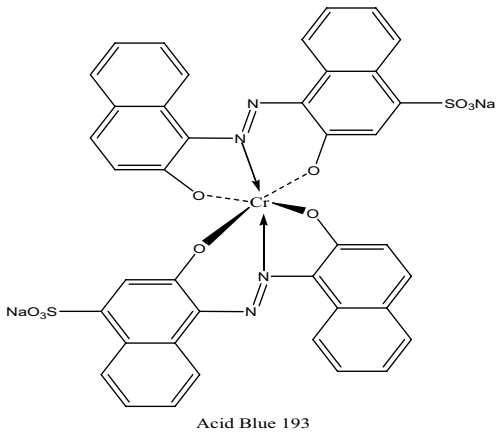
2 Materials and methods

2.1 Material collection and biosorbent preparation

The acid blue 193 dye was purchased from Synthesia Company, Czech Republic and was used as received. Table 1 presents the dye structure, its maximum wavelength, and molecular weight. Other reagents used in the study: sodium hydroxide, sodium carbonate, nitric acid, HCl, ethyl alcohol, and acetone were all laboratory-grade chemicals (Merck, Germany).

Apricot was purchased from a fruit shop in Cairo metropolis, Egypt. The seeds were isolated and washed several

Table 1 Properties of the acid blue 193 dye

Properties	
Molecular formula	$C_{40}H_{22}CrN_4Na_2O_{10}S_2$
Maximum wavelength	~580 nm
Molecular weight (kg/mol)	880.7
CAS Number	12392-64-2
Structure	 Acid Blue 193

times with hot water to get rid of adherent fruit residues, dust, and suspended matter. Afterwards, the seed shells were manually isolated using mortar, oven-dried for 5 h at 105 °C and then grind to fine particle size (~50–125 µm) to obtain the desired apricot seed shell adsorbent powder (*ASP*). The corresponding physical and chemical characteristics of this material are summarized in Table 2. The stages involved during the biosorbent preparation are presented in Scheme 1.

2.2 Instrumental characterization procedures

2.2.1 Fourier transform infrared spectroscopy (FTIR)

The pre-and post-adsorption FTIR spectra of the *ASP* sample were determined using Perkin–Elmer spectrophotometer from 4000 to 400 cm^{-1} using KBr discs containing ~5–10 mg of sample in ~300 mg of KBr.

2.2.2 Scanning electron microscopy (SEM) and energy dispersion X-ray (EDX)

The SEM micrograph of the *ASP* sample was obtained (after overlaying the sample with a thin layer of gold using a diode sputter unit) on a scanning electron microscope (model JEOL-JSM-5600), at an accelerating voltage of 25.0 kV. Elemental analysis of the samples was obtained using an EDX spectrometer (Oxford Instruments 6587 EDX detector), attached to the JEOL-JSM-5600 unit used for SEM analysis.

2.2.3 X-ray diffraction (XRD)

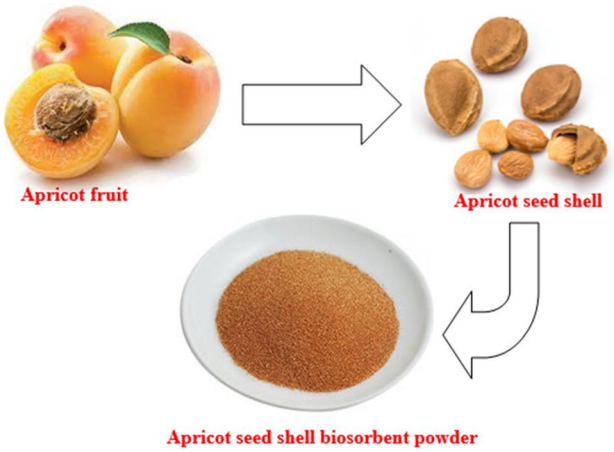
The XRD patterns were obtained on a PANalytical diffractometer (X'Pert PRO) in continuous scanning mode using a Cu tube (in the reading range of 2 to 80°).

2.2.4 Brunauer–Emmett–Teller (BET) surface area

The nitrogen gas adsorption-desorption method was adopted for the Brunauer–Emmett–Teller (BET) and Barrett, Joyner, and Halenda (BJH) surface area measurement. During the surface area measurement, the automated Belsorp Max surface area analyzer operated at 77 K was used. Before the analyses, an accurate mass of the *ASP* sample was obtained and was further degassed for 2 h at 200 °C.

Table 2 Physical and chemical characteristics of apricot seed shell powder

Parameters	
Bulk density (g/cm^3)	0.35
Porosity (%)	49.99
pH	2.0
pH_{PZC}	7.3



Scheme 1 Schematic representation of the biosorbent preparation stages

2.3 Determination of the pH at zero charge (pH_{pzc})

A total of 100 ml of 0.01N NaCl solution was prepared and added to eleven (11) different Erlenmeyer flasks. The initial pH values of the flasks were respectively tuned (between pH 2.0 and pH 12.0) using 0.01N NaCl solution. After the constant value of pH initial had been reached, 0.1 g of adsorbent sample was added to each Erlenmeyer flask. The solution pH was measured after 24 h and noted as pH_{final}. Then, a plot of the change in pH, ΔpH (pH_{final}-$pH_{initial}$) against $pH_{initial}$ was generated and the pH_{pzc} of the *ASP* sample was marked off at the point where the ΔpH is zero.

2.4 Batch adsorption studies

In an equilibrium experiment, 0.2 g of the *ASP* sample and 100 ml of an aqueous dye solution of varying concentrations: 10–100 mg/L, were placed in a 125 ml glass stoppered flask and stirred for 2 h using a shaking water bath operated at 200 rpm at 30 °C. Test samples were intermittently withdrawn from the shaker, and the dye solution was separated from the adsorbent by centrifugation. Dye concentration in the supernatant solution was measured with a Shimadzu UV/Visible Spectrophotometer at ~580 nm wavelength. A concentration calibration curve was constructed by plotting the absorbance versus the concentration of standard dye solutions ranging from 0 to 100 mg/L. The equilibrium adsorption capacity, q_e (mg/g), of the *ASP* sample was evaluated from Eq. (1).

For kinetic evaluation, test samples were intermittently withdrawn at 5 min intervals within a time range of 0–180 min. The instantaneous adsorption capacity, q_t (mg/g), of the *ASP* sample was evaluated from Eq. (2). All adsorption and kinetic experiments were carried out in duplicate and the

mean values of q_e were reported. NB: All the terms in the equations are properly defined in the nomenclature.

$$q_e = \frac{(C_o - C_e) * V}{W} \quad (1)$$

$$q_t = \frac{(C_o - C_t) * V}{W} \quad (2)$$

2.5 Adsorption isotherm and kinetic studies

Process modeling is an important aspect of any scientific study [29]. The adsorption isotherm study provides insight into the nature of the adsorbate-adsorbent interaction, while the kinetics study elucidates the time dependence of the adsorption system. In this study, the nonlinear isotherm and kinetics model whose equations are presented in Table 3 were employed.

2.6 Error analysis

To evaluate the correlation between the experimental data and model-predicted data, the average relative error (ARE), average percentage error (APE), sum squares error (ERRSQ/SSE), hybrid fraction error function (hybrid), Marquardt's percent standard deviation (MPSD), and nonlinear chi-square test (χ^2) were adopted. The mathematical equations of these error models and the equation of the coefficient of determination (R^2) have been previously reported by the authors [30–32]. Using the error models, the different error values obtained for a given isotherm/kinetic model prediction are further normalized following the procedure reported by Dubey et al. [33] and Hashem et al. [34]. Thus, the SNE value is a summation of the quotients obtained by dividing through the individual error values with the single largest error value for each isotherm/kinetics model. Consequently, the best fit model is determined based on the magnitude of its sum of normalized error values, SNE and the lower the SNE-value, and the better the model fitting to the experimental data.

Table 3 Nonlinear isotherm, kinetics, and mechanistic model equations

	Equation	Eq. no
Isotherm models		
Langmuir	$q_e = \frac{q_{max} K_L C_e}{1+K_L C_e}$	(3)
Freundlich	$q_e = K_F C_e^{1/n}$	(4)
Temkin	$q_e = \frac{RT}{b_T} \ln (K_T C_e)$	(5)
Dubinin–Radushkevich	$q_e = q_D * \exp\left\{-B_D\left[RT\left(1+\frac{1}{C_e}\right)\right]^2\right\}$	(6)
Kinetics model		
Pseudo-first-order	$q_t = q_e[1 - exp(-K_1 t)]$	(7)
Pseudo-second order	$q_t = \frac{K_2 \cdot q_e^2 \cdot t}{1+K_2 \cdot q_e \cdot t}$	(8)
Mechanistic model		
Intraparticle diffusion	$q_t = K_{id}\sqrt{t} + C$	(9)

3 Results and discussions

3.1 Biosorbent sample characterization

3.1.1 Fourier transform infrared spectroscopy (FTIR) analysis

The spectra of raw and spent *ASP* samples (Fig. 1) present numerous peaks which suggest the complex nature of its surface chemistry. To limit the complexity and make for a better understanding, only the prominent peaks were identified and assigned to the relevant functional groups (Table 4). Incidentally, both samples presented similar functional groups and their distinction was only reflected in the associated wavenumbers. The slight difference between the pre-and post-biosorption wavenumbers is a consequence of the adsorptive interaction between the anionic dye molecules and the *ASP* surface [28, 35]. The broad peak of –OH groups observed around 3300 cm^{-1} could have originated from the alcohols, phenols, and carboxylic acid content of the *ASP* [36]. The symmetric aliphatic (-CH_2) stretching vibration and aromatic carbonyl/carboxyl group could have respectively originated from the organic acid and polyphenol content of the biosorbent [37]. The alcoholic and carboxylic acid groups which confirm the presence of lignin are represented around 1027 cm^{-1} [38]. Thus, the FTIR investigation informs of the presence of carboxyl and hydroxyl biopolymer groups which could donate proton for anionic dye molecules.

3.1.2 Scanning electron microscopy-energy dispersion x-ray (SEM-EDX) analysis

The SEM micrograph of the raw *ASP* (Fig. 2a) had a characteristic irregular surface with extensive surface porosity. The numerous surface micropores confer the *ASP* biosorbent with adequate morphology for dye biosorption. In the post-adsorption micrograph (Fig. 2b), these micropores were conspicuously absent and a bright surface layer of adsorbed dye was also observed. This development is due to the probable occupation of these micropores by the adsorbed dye molecules. The successful loading of the dye molecules onto the *ASP* sample was further confirmed by energy-dispersive X-ray (EDX) analysis (Fig. 3). Accordingly, the presence of a chromium signal on the elemental

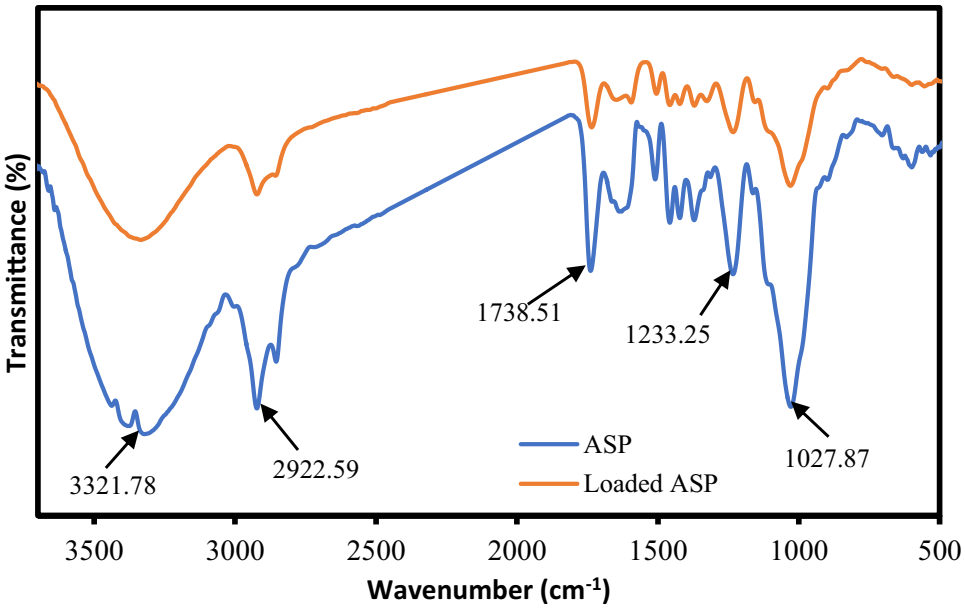


Fig. 1 The FTIR spectra of the raw and loaded *ASP* samples

Table 4 The prominent peaks on pre-and post-biosorption *ASP* samples

Pre-adsorption values		Post-adsorption values		Assigned functional group
Wavenumber (cm^{-1})	Intensity (%)	Wavenumber (cm^{-1})	Intensity (%)	
3321.78	36.07	3334.32	64.28	–OH stretching vibrations
2922.59	41.11	2934.59	73.25	Asymmetric $–CH_2$ stretching
1745.51	68.19	1728.66	86.45	–C=O stretching vibration
1233.25	67.54	1228.25	85.51	Symmetric C–H vibration
1027.87	41.44	1029.80	74.95	C–OH stretching vibration

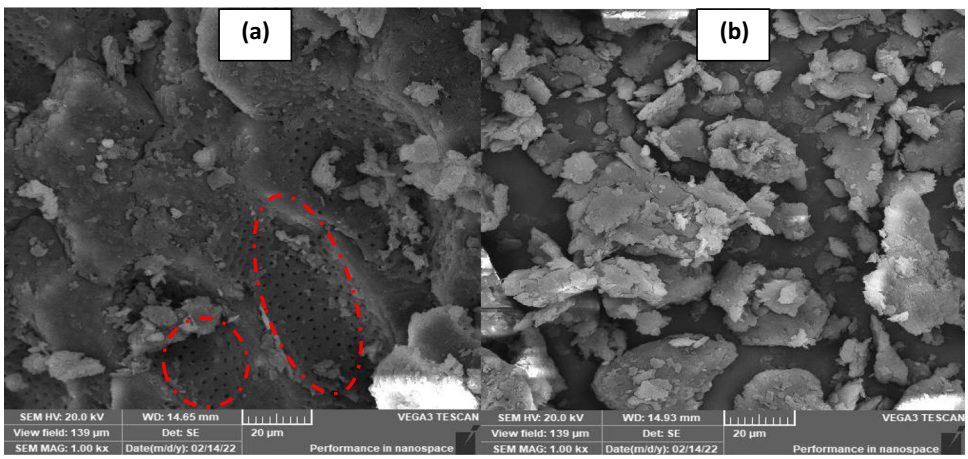


Fig. 2 SEM image of **a** raw and **b** dye-loaded *ASP*

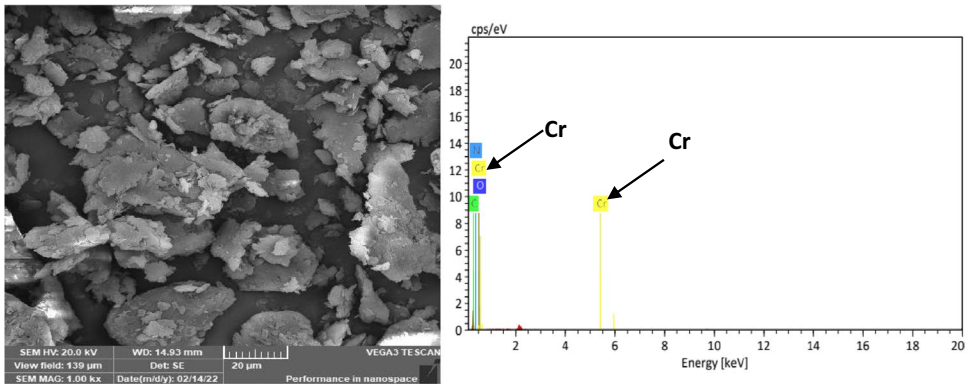


Fig. 3 SEM-EDX result for dye-loaded *ASP*

mapping spectra is a clear indication of successful dye uptake, since chromium is the prominent constituent of the acid blue 193 dye.

3.1.3 X-ray diffraction (XRD) analysis

The X-ray diffraction (XRD) facilitates understanding of the physical properties of different solids material and biosorbents [39]. The pre-adsorption XRD pattern (Fig. 4a) showed two peaks: an intense broad peak at 22.71° (2θ) and another sharp peak at 44.70° (2θ). The observed broadening of the peak at 22.71° (2θ) is an indication of poor crystallinity [40]. After adsorption (Fig. 4b), the sharp peak previously observed in the raw *ASP* sample significantly diminished and left only a miniature trace at 44.65° (2θ). Hence, the cellulose that is present in the *ASP* biosorbent existed mostly in amorphous and micro-fibrillated nature [41]. Consequently, a long range of amorphous/diffuse diffraction patterns was generally observed in both the pre-and post-adsorption sample. This could be a result of the high presence of amorphous hemicellulose, lignin, and other fibrous contents in the respective sample.

3.1.4 Brunauer–Emmett–Teller (BET) analysis

The BET surface area and pore size distribution of the ASP sample were analyzed to determine their influence on the dye uptake. The surface area, pore volume, and pore radius were recorded as 97.493 m^2/g, 0.0691 cm^3/g, and 1.922 nm, respectively. This surface area value indicates good porosity and was found to be larger than 1.3 m^2/g, 5.36 m^2/g, and 4.01 m^2/g recorded for apricot seed shell [28], *N. diderrichii* seed [42] and *M. oleifera* seed [43], respectively. Furthermore, the average pore radius of the biosorbent is less than 2 nm and hence they fall within the microporous range following the IUPAC pore distribution classification [44, 45]. This conclusion we made regarding the pore radius corroborates the earlier presence of micropores observed from the SEM micrograph of the raw *ASP* (section 3.1.2).

3.1.5 Point of zero charge (pH_{PZC}) analysis

The extent of uptake of charged solutes like our anionic acid blue 193 dye is always a function of the point of zero charge (pH_{PZC}) value of the biosorbent [46]. The pH_{PZC} value refers to the pH at which the net surface charge of a given biosorbent is zero [12]. Thus, for enhanced electrostatic interaction, cationic solutes are better adsorbed when the solution pH is greater than the pH_{PZC} value. Similarly, when the solution pH is less than the pH_{PZC} value, uptake of anionic solutes is favored [47]. According to the plot shown in Fig. 5, the pH_{PZC} of the *ASP* sample was experimentally determined as pH 7.3. This finding points to the fact that the biosorption of anionic acid blue 193 dye will be favorable at acidic pH ranges ($pH < pH_{PZC}$). The

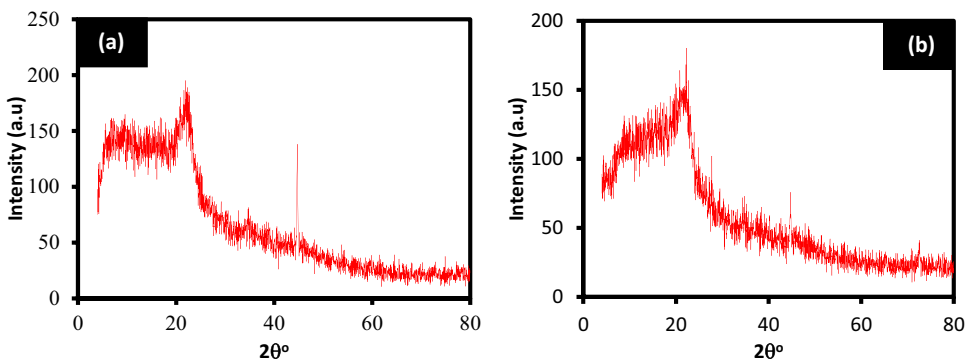


Fig. 4 The XRD spectra of the **a** raw and **b** loaded *ASP* samples

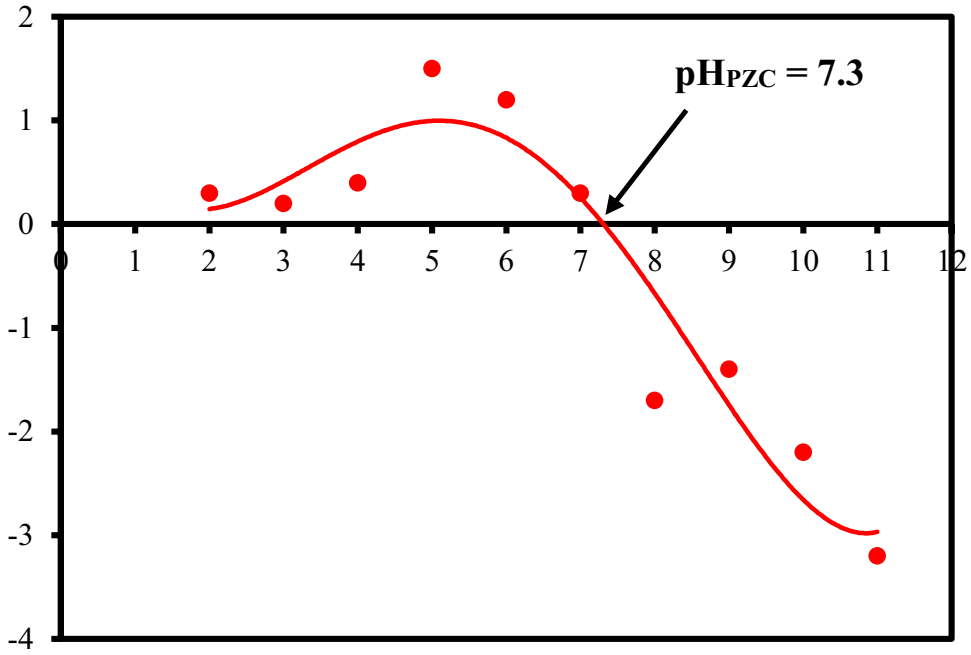


Fig. 5 pHpzc of *ASP* biosorbent

authenticity of such assertion was further tested during the study on the effect of solution pH on the dye uptake capacity.

3.2 Effect of process variables on biosorption capacity

3.2.1 Effect of pH

Solution pH is an important control variable during solute uptake. In this study, the effect of solution pH on the *ASP* biosorption capacity was investigated within the range of pH 2.0 to 10.0 at a constant 40 mg/L dye concentration using 0.2 g/L of biosorbent. The experimental finding was processed, and the result is presented in Fig. 6. With due recourse to the pH_{PZC} value for the *ASP* biosorbent earlier obtained and discussed in section 3.1.5, an improved biosorbent-adsorbate electrostatic attraction and repulsion are expected to occur at pH < pH 7.3 and pH > pH 7.3, respectively. This assertion explains the consistent increase in the biosorption capacity with every slightest increase in solution acidity. Thus, the maximum (26.47 mg/g) and minimum (10.0 mg/g) dye uptake were achieved at pH 2.0 and 10.0. Therefore, electrostatic interaction is regarded as the possible mechanism in the study.

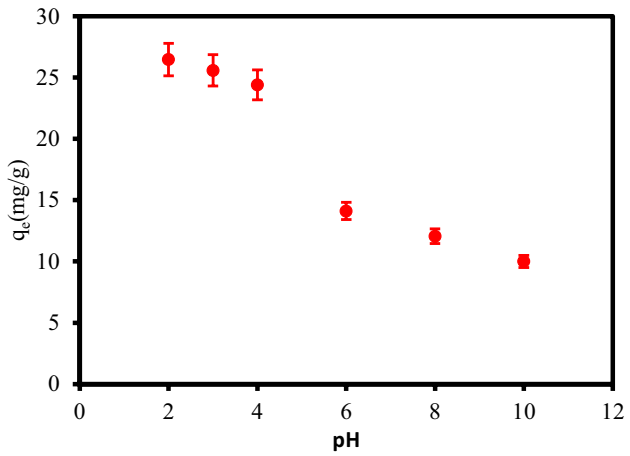


Fig. 6 The plot of temperature against biosorption capacity (q_e, mg/g)

3.2.2 Effect of temperature

The effect of temperature on the biosorption capacity was investigated and the experimental finding is presented in Fig. 7. Notably, there was a steep decrease in the uptake capacity with an initial 10 °C rise in temperature (from 30 to 40 °C). A consistent decline in dye molecule uptake persisted with further temperature rise. This observation shows the occurrence of an exothermic process and indicates weak adsorptive (physisorption) interaction. Based on the foregoing, it is however believed that with an increase in temperature comes an increase in the dye molecules' kinetic energy and a decrease in the boundary layer thickness [48]. As a result, the weak physisorption forces weaken and in line with Le-Chatelier's principle, the desorption of the earlier adsorbed dye molecules is thus favored.

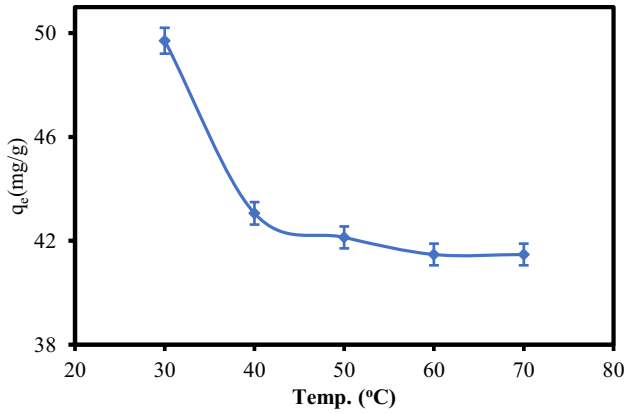


Fig. 7 The plot of temperature (°C) against biosorption capacity (q_e, mg/g)

3.2.3 Effect of biosorbent dosage

The investigation was carried out at 40 mg/L initial dye concentration, pH 2.0, and varying *ASP* dosages (0.2 to 2.0 g/L). Based on the experimental finding presented in Fig. 8, the increase in the biosorbent dose led to a consistent decrease in the amount of dye adsorbed (q_e, mg/g), Notably, the q_e, mg/g value dropped from 25.29 mg/g (at 0.2 g/L) to 5.75 mg/g (at 2.0 g/L). At 0.2 g/L, there is a higher coefficient of *ASP* biosorbent utilization such that the available surface active sites could reach their saturation point [49]. Also, the effect of adsorbate concentration flux on biosorbent is quite large at such a low dosage [50]. Conversely, at a higher dosage of 2.0 g/L, there is an increment in the number of available active sites which results in their progressive unsaturation. Also, there is the possibility of agglomeration and clogging of *ASP* particles and this will further diminish the overall biosorbent surface area [51]. Similarly, observation was made in existing literature [52–54].

3.2.4 Effect of contact time and initial dye concentration

The combined effects of contact time (0–240 min) and initial dye concentration (20 and 40 mg/L) on the biosorption capacity were investigated. The result of the experiment is presented in Fig. 9. The biosorption capacity was found to increase from 0 to 21.42 mg/g (at 20 mg/L concentration) and 0 to 34.41 mg/g (at 40 mg/L concentration) within the first 5 min of biosorption. After the first 5 min, the rate of biosorption capacity increase was slower but persistent for both initial dye concentrations until equilibrium was finally attained at 120 min. The initial rapid dye uptake experienced at the onset of biosorption is related to the high presence of unsaturated active sites which is synonymous with a high biosorbent utilization coefficient [11]. The observed decline in the uptake rate as the contact time extended followed by an eventual equilibration is a result of the continued occupation of the available active sites until saturation. Furthermore, it was observed that the extent of dye uptake varies directly with the initial concentration. For instance, maximum dye uptake of 41.17 and 24.71 mg/g was respectively recorded at 20 mg/L and 40 mg/L initial concentrations. This observation is attributed to an increase in concentration gradient experienced at a higher concentration which masks the effect of mass transfer resistance [55].

3.3 Biosorption modeling

3.3.1 Isotherm modeling

An efficient isotherm modeling provides insight into the capacity of a given biosorbent to adsorb a unit mass of a

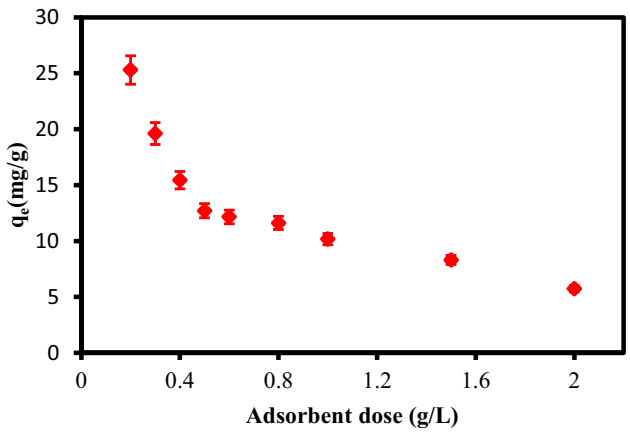


Fig. 8 The plot of biosorbent dosage (g/L) against biosorption capacity (q_e, mg/g)

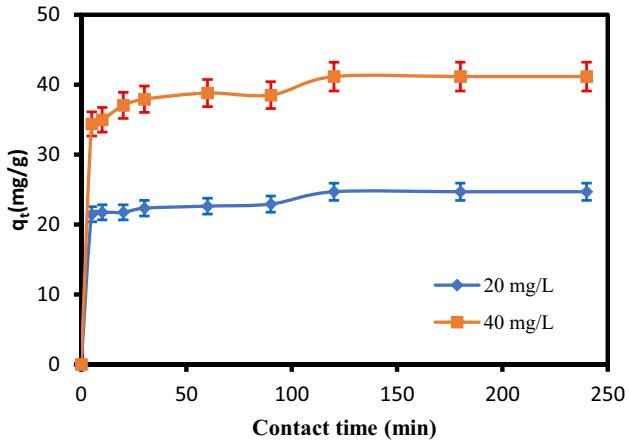


Fig. 9 The plot of contact time (min) against biosorption capacity (q_e, mg/g) at varying initial dye concentrations

solute at specified operating conditions. Consequently, the experimental equilibrium data were fitted to four (4) nonlinear isotherm models' equations, namely the Langmuir (Eq. 3), Freundlich (Eq. 4), Temkin (Eq. 5), and Dubinin–Radushkevich (D–R) (Eq. 6) isotherms. Meanwhile, the associated model parameters, coefficient of determination (R^2), and the sum of normalized error (SNE) values (section 2.6) are given in Table 5. Since the model parameters were iteratively generated via a nonlinear regression approach, the associated plots were very dispensable and hence, not supplied.

The Langmuir equation [56] considers monolayer coverage, the existence of sorption sites with uniform energy and no lateral between solutes bound to adjacent sites as its fundamental hypotheses. The Langmuir model has two dimensionless constants: the R_L and K_L values. The R_L values indicate the favorability ($0 < R_L < 1$), unfavourability ($R_L > 1$), linearity ($R_L = 1$), or irreversibility ($R_L = 0$) of a given system [57, 58]. Accordingly, the present sorption, with an R_L value of 0.029, is considered favorable. Also, the K_L value which is both positive and greater than unity shows an improved sorption affinity [59], as informed by the large q_{max} value of 104.65 mg/g. The Freundlich equation is most applicable for interpreting sorption onto heterogeneous surfaces or surfaces with active sites of varying affinities [60, 61]. The favorability and extent of biosorption affinity are elucidated from the magnitude of the n_F ($1 < n_F < 10$) and the K_F ($K_F > 1$) values. The n_F and K_F values of 1.86 and 7.53 respectively indicate a favorable process and improved adsorptive interaction [35, 62]. Just like the Langmuir, the Temkin model postulates a monolayer adsorbate distribution but on heterogeneous sites with consistent binding energy distribution and biosorbent-solute interaction [32, 63]. The model further assumes that the adsorption heat linearly depends on surface coverage. Thus, a positive Temkin (b_T) value of 296.63 J/mol, which was far greater than unity, is indicative of a favorable process. As an empirical model, the D-R model has no assumptions but the magnitude of its mean sorption energy E (kJ/mol) parameter suggests whether the process is physisorption (E < 8 kJ/mol), physicochemical (8 <E < 16 kJ/mol) or chemisorption (E > 16 kJ/mol). The D-R mean sorption free energy (E) value of 144.33 kJ/mol obtained in the study suggests chemisorption [64] but this result may not be a true reflection of the nature of the system because the D-R model was not the model of best fit.

Consequently, the validity of the respective isotherm models was evaluated solely from the magnitude of the SNE value, since all the models showed high R^2 values ($R^2 > 0.9$). It is therefore concluded that the Temkin model with the lowest SNE value of 1.151 gave the best model description. This suggests a monolayer solute distribution but on heterogeneous *ASP* sites with consistent binding energy and biosorbent-solute interaction [34, 65].

Table 5 Isotherm model parameters

Langmuir	Freundlich	Temkin	Dubinin–Radushkevich
q_{max} = 104.65	n_F = 1.86	A_T = 8.44	q_D = 63.99
k_L = 3.03	K_F = 7.53	b_T = 296.63	B_D = 2.40E-05
R_L = 0.029	R^2 = 0.996	R^2 = 0.935	R^2 = 0.984
R^2 = 0.997	SNE = 1.391	SNE = 1.151	E = 144.33
SNE = 1.420			SNE = 1.262

3.3.2 Kinetics modeling

The kinetics study is necessary for evaluating the solute mass transfer rate and its associated mechanisms during the biosorption process [66]. Dedicated models are often applied for such investigation and in this study, the pseudo-first-order (PFO) and pseudo-second-order (PSO) kinetics models were applied. Our choice of kinetics model was informed by the fact that the PFO and PSO models have wide applications in studies involving liquid-solid interactions. Fundamentally, the PFO model assumes direct proportionality between the sorption rate and the difference between equilibrium (q_e, mg/g) and instantaneous (q_t, mg/g) biosorption capacities, while the PSO model assumes a second-order uptake rate to the available surface sites [67]. However, the relevant parameters for PFO and PSO models, their coefficient of determination, and error values as presented in Table 6 were iteratively estimated using the SOLVER function of the Microsoft Excel v2016 software. Also, the generated model plots are presented in Fig. 10.

Based on the previous studies [68, 69], the prediction accuracy of the experimental q_e, mg/g by the PFO model is always inferior to that of the PSO. According to q_e, mg/g values obtained for both models at 20 and 40 mg/L initial concentrations (Table 6), the aforementioned assertion applied to our study. Furthermore, the reaction rate constants

Table 6 Kinetic and mechanistic model parameters

PFO	PSO	Intraparticle diffusion
20 mg/L		
q_e = 22.94	q_e = 23.90	k_{id} = 0.24
k_1 = 0.549	k_2 = 0.071	C = 20.92
R^2 = 0.997	R^2 = 0.998	R^2 = 0.999
SNE = 2.122	SNE = 2.167	
40 mg/L		
q_e = 38.82	q_e = 39.69	k_{id} = 0.47
k_1 = 0.417	k_2 = 0.019	C = 34.81
R^2 = 0.997	R^2 = 0.998	R^2 = 0.999
SNE = 1.627	SNE = 1.673	

NB: $q_{e, exp}$ = 24.706 mg/g (for 20 mg/L) and 41.176 mg/g (for 40 mg/L)

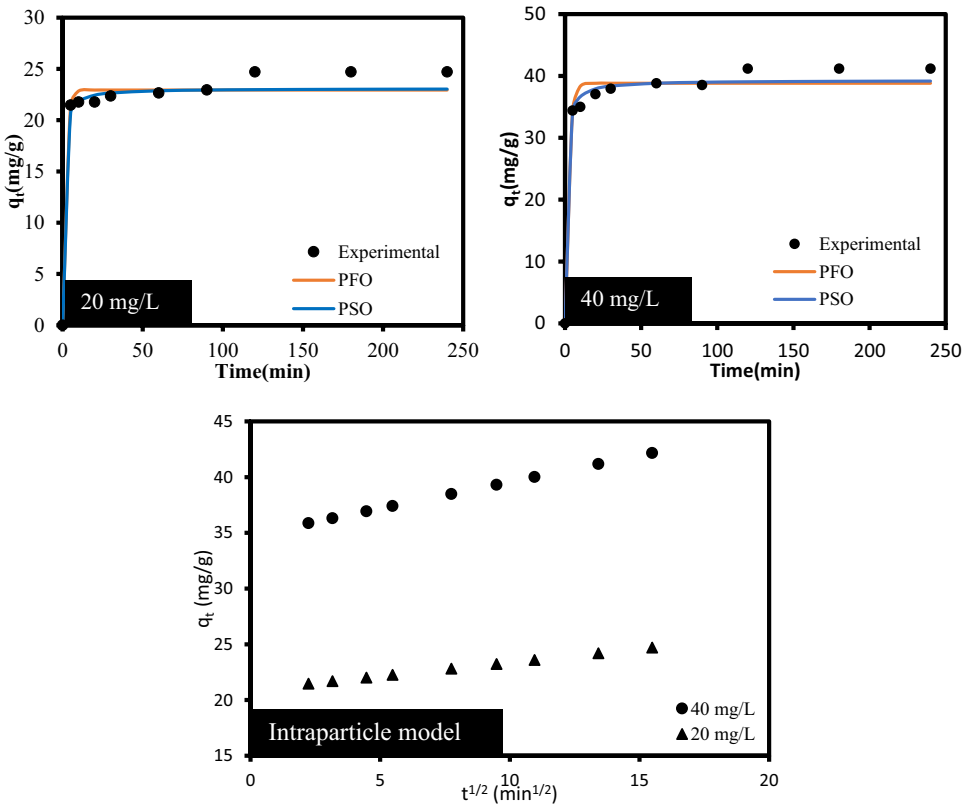


Fig. 10 Kinetics plots of PFO, PSO and intraparticle diffusion model at varying initial dye concentrations

for both models (k_1 and k_2) generally decreased with increasing initial dye concentration [70, 71]. Noting that the inverse of the respective rate constants ($1/k_n$; $n = 1$ or 2) gives the time scale for equilibrium attainment during uptake, the solute uptake rate gets slower with an increase in initial dye concentration due to the ionic competition effect. Beyond the deductions made from the generated parameters, the models' validity was further evaluated solely from the magnitude of the SNE value, since both models depicted high R^2 values ($R^2 > 0.9$) for all initial dye concentrations. Therefore, it could be concluded that the PFO model with the lowest SNE value of 2.122 (for 20 mg/L concentration) and 1.627 (for 40 mg/L concentration) gave the best model description in both systems. This suggests predominant physisorption and further corroborates our findings from the study on the effect of temperature (section 3.2.4).

To ascertain the main solute mass transfer mechanism, the experimental kinetic data were modeled with the intraparticle diffusion model. The associated linear plot of q_t versus $t^{1/2}$ obtained from the model is shown in Fig. 10. Consequently, model parameters (k_{id} and C) together with the R^2 values obtained at 20 and 40 mg/L initial concentrations are presented in Table 6. The value of the intraparticle diffusion rate constant the k_{id} was found to increase from 0.24 to 0.47 mg/g*$min^{1/2}$ as the initial concentration increased from 20 to 40 mg/L. This observation is attributed to the increased adsorption driving force occasioned by the increase in dye concentration and further confirms the occurrence of improved intraparticle diffusion through *ASP* at increasing dye concentration. Similarly, the intercept, C, which represents the boundary layer effect also increased from 20.92 (at 20 mg/L concentration) to 34.81 (at 40 mg/L concentration). This finding signifies a greater contribution of interfacial/surface adsorption (with increasing adsorbate concentration) to the overall rate-limiting step.

3.4 Comparison of adsorption capacities of various adsorbents towards acid blue dye

The maximum adsorption capacity for acid blue 193 ions onto *ASP*, according to the Langmuir isotherm model, was 104.65 mg g^{-1}. This relatively large adsorption capacity value is an indication of the strong affinity between the *ASP* and the acid blue 193 molecules as compared to the result of the previous studies which are shown in Table 7.

4 Conclusion

Apricot seed shell powder (*ASP*) has been utilized as adsorbent material for the adsorption of acid blue 193 from contaminated water. The ability of *ASP* to adsorb aid blue 193 was investigated by using the batch adsorption procedure. It was shown that the adsorption capacity of acid blue 193

Table 7 Comparison of adsorption capacities of various adsorbents for acid blue dye

Types of adsorbents	Adsorption capacity (mg/g)	Ref
Fly ash	10.93	[72]
Na–bentonite	67. 1	[73]
Red pine sawdust	54.16	[74]
Spent *ribulu sterrestris*	93.00	[75]
Phosphoric acid treated rubber leaf powder	28.09	[76]
Synthesized polymeric nanocomposites	55.55	[77]
Carbon nanotubes	86.91	[78]
Apricot seed shell powder (*ASP*)	104.65	Present study

onto *ASP* was affected by adsorbent dose, pH, contact time, and dye concentration in the solution. The characteristics of the prepared biosorbent were extensively elucidated in line with the results obtained from the FTIR, SEM-EDX, XRD, surface area, and pH_{PZC} examination. The adsorption equilibrium data were analyzed using a suite of two-parameter (Langmuir, Freundlich and Temkin, Dubinin–Radushkevich) isotherm models, while the respective models' goodness of fit was determined using the nonlinear error functions. Similarly, the adsorption kinetics data were analyzed using two kinetics models and one mechanistic model. However, the equilibrium and kinetics data were well described by the Temkin and pseudo-first-order models, respectively. This suggests monolayer solute physisorption distribution on heterogeneous *ASP* sites with consistent binding energy and biosorbent-solute interaction. Thus, *ASP* is an effective adsorbent for the removal of acid blue 193 from contaminated water. However, just like all low-cost biosorbents, much work is still required in the area of predicting their adsorptive performance and mechanism using real industrial effluents at an industrial scale under specific operating conditions.

Nomenclature C_o: initial acid blue 193 dye concentration (mg L^{-1}); C_e: equilibrium acid blue 193 dye concentration (mg L^{-1}); W: mass of *ASP* used (g); V: volume of acid blue 193 dye solution (0.1 L); q_D: D-R constant (mol g^{-1}); B_D: mean sorption free energy E (kJ mol^{-1}) per molecule of sorbate; K_T: Temkin equilibrium binding constant (L mol^{-1}); b_T: Temkin constant that is related to the adsorption heat (J mol^{-1}); R: universal gas constant (8.314 J K^{-1} mol^{-1}); T: temperature (K); q_e: amount of adsorbate adsorbed per gram of adsorbent (mg g^{-1}) at equilibrium; q_t: amount of adsorbate adsorbed per gram of adsorbent (mg g^{-1}) at an instant; K_F: Freundlich isotherm constant [(mg g^{-1}) (L/mg)$^{1/n}$]; n_F: Freundlich adsorption intensity; K_L: Langmuir constant (L g^{-1}); R_L: Langmuir's dimensionless constant (separation factor); q_{max}: Langmuir maximum adsorption capacity (mg g^{-1}); k_1: pseudo-first-order rate constant (min^{-1}); k_2: pseudo-second-order rate constant (g.mg^{-1} min^{-1}); k_T: Temkin initial adsorption rate (mg (g min) $^{-1}$); b_T: Temkin constant which is related to the extent of surface coverage (g mg $^{-1}$); k_{id}: intra-particle diffusion rate constant(mg g $^{-1}$ min $^{1/2}$); $t^{1/2}$: half-adsorption time, (g min $^{-1}$ mg); α: initial adsorption rate (mg. $g^{-1}min^{-1}$); β: desorption constant (g.mg^{-1}) during any experiment

Author contribution A. Hashem: conceptualization, project administration, data curation, supervision, writing — original draft, and writing — review and editing. Chukwunonso O. Aniagor: conceptualization, project administration, data curation, supervision, writing — original draft, and writing — review and editing. Osama M. Morsy: experimentation, formal analyses, data curation, and writing — review and editing. A. Abou-Okeil: experimentation, formal analyses, data curation, and writing — review and editing. A.A. Aly: investigation, formal analyses, data curation, and writing — review and editing.

Availability of data and material

Funding Open access funding provided by The Science, Technology & Innovation Funding Authority (STDF) in cooperation with The Egyptian Knowledge Bank (EKB).

Data availability All data generated or analyzed during this study are included in this published article.

Declarations

Ethics approval Not applicable.

Conflict of interest The authors declare no competing interests.

Open Access This article is licensed under a Creative Commons Attribution 4.0 International License, which permits use, sharing, adaptation, distribution and reproduction in any medium or format, as long as you give appropriate credit to the original author(s) and the source, provide a link to the Creative Commons licence, and indicate if changes were made. The images or other third party material in this article are included in the article's Creative Commons licence, unless indicated otherwise in a credit line to the material. If material is not included in the article's Creative Commons licence and your intended use is not permitted by statutory regulation or exceeds the permitted use, you will need to obtain permission directly from the copyright holder. To view a copy of this licence, visit http://creativecommons.org/licenses/by/4.0/.

References

1. Sen TK, Afroze S, Ang H (2011) Equilibrium, kinetics and mechanism of removal of methylene blue from aqueous solution by adsorption onto pine cone biomass of Pinus radiata. Water Air Soil Pollut 218(1):499–515
2. Yagub MT, Sen TK, Ang H (2012) Equilibrium, kinetics, and thermodynamics of methylene blue adsorption by pine tree leaves. Water Air Soil Pollut 223(8):5267–5282
3. Hashem A, Aniagor CO, Abdel-Halim E, Amr A, Farag S, Aly A (2022) Instrumental characteristics and acid blue 193 dye sorption properties of novel lupine seed powder. Cleaner Chem Eng 2:100011
4. Chimupala Y, Phromma C, Yimklan S, Semakul N, Ruankham P (2020) Dye wastewater treatment enabled by piezo-enhanced photocatalysis of single-component ZnO nanoparticles. RSC Adv 10(48):28567–28575

5. Zhu G, Fang H, Xiao Y, Hursthouse AS (2020) The application of fluorescence spectroscopy for the investigation of dye degradation by chemical oxidation. J Fluoresc 30(5):1271–1279
6. Dolatabadi M, Świergosz T, Ahmadzadeh S (2021) Electro-Fenton approach in oxidative degradation of dimethyl phthalate-the treatment of aqueous leachate from landfills. Sci Total Environ 772:145323
7. Hashem A, Hussein HA, Sanousy MA, Adam E, Saad EE (2011) Monomethylolated thiourea - sawdust as a new adsorbent for removal of Hg (II) from contaminated water: equilibrium kinetic and thermodynamic studies. Polym Plast Technol Eng 50(12):1220–1230
8. Zou H, Ma W, Wang Y (2015) A novel process of dye wastewater treatment by linking advanced chemical oxidation with biological oxidation. Arch Environ Prot 41(4):33–39
9. Kalipci E, Sahinkaya S, Dortkol M, Aras S (2016) Decolorization of basic textile dyes using a novel adsorbent modification method: ultrasonic-acid modification. Int J Environ Res 10(1):31–40
10. Abbasi S, Ahmadpoor F, Imani M, Ekrami-Kakhki M-S (2020) Synthesis of magnetic Fe3O4@ ZnO@ graphene oxide nanocomposite for photodegradation of organic dye pollutant. Int J Environ Anal Chem 100(2):225–240
11. Aniagor CO, Afifi M, Hashem A (2021) Heavy metal adsorptive application of hydrolyzed corn starch. J Polym Res 28(11):1–10
12. Mohamed LA, Aniagor CO, Taha GM, Abou-Okeil A, Hashem A (2021) Mechanistic investigation of the mass transfer stages involved during the adsorption of aqueous lead onto Scopulariopsis brevicompactum fungal biomass. Environ Challenges 5:100373
13. Dolatabadi M, Naidu H, Ahmadzadeh S (2021) A green approach to remove acetamiprid insecticide using pistachio shell-based modified activated carbon; economical groundwater treatment. J Clean Prod 316:128226
14. Rangabhashiyam S, Anu N, Selvaraju N (2013) Sequestration of dye from textile industry wastewater using agricultural waste products as adsorbents. J Environ Chem Eng 1(4):629–641
15. Menkiti M, Aniagor C (2018) Parametric studies on descriptive isotherms for the uptake of crystal violet dye from aqueous solution onto lignin-rich adsorbent. Arab J Sci Eng 43(5):2375–2392
16. Anastopoulos I, Kyzas GZ (2014) Agricultural peels for dye adsorption: a review of recent literature. J Mol Liq 200:381–389
17. Salleh MAM, Mahmoud DK, Karim WAWA, Idris A (2011) Cationic and anionic dye adsorption by agricultural solid wastes: a comprehensive review. Desalination 280(1-3):1–13
18. Mahmoodi NM, Arami M, Bahrami H, Khorramfar S (2010) Novel biosorbent (Canola hull): surface characterization and dye removal ability at different cationic dye concentrations. Desalination 264(1-2):134–142
19. Libing W (2008) Progress of exploitation and utilization research of wild apricot. J Zhejiang For Sci Technol 28(6):76–80
20. Elmenofy HM, Okba SK, Salama A-M, Alam-Eldein SM (2021) Yield, fruit quality, and storability of 'canino'apricot in response to aminoethoxyvinylglycine, salicylic acid, and chitosan. Plants 10(9):1838
21. Yüksel Ş, Orhan R (2019) The removal of Cr (VI) from aqueous solution by activated carbon prepared from apricot, peach stone and almond shell mixture in a fixed-bed column. Arab J Sci Eng 44(6):5345–5357
22. Buyukada M, Aydogmus E (2018) Utilization of apricot seed in (co-) combustion of lignite coal blends: numeric optimization, empirical modeling and uncertainty estimation. Fuel 216:190–198
23. Tavakoli-Hosseinabady B, Ziarati P, Ballali E, Umachandran K (2018) Detoxification of heavy metals from leafy edible vegetables by agricultural waste: apricot pit shell. J Environ Anal Toxicol 8(1):548
24. Kahraman S, Yalcin P, Kahraman H (2012) The evaluation of low-cost biosorbents for removal of an azo dye from aqueous solution. Water Environt J 26(3):399–404
25. Ismail AM, Loganathan M, Theodor PA (2012) Effect of bioadsorbents in removal of colour and toxicity of textile and leather dyes. J Ecobiotechnol 4(1):1–10
26. Ammar F, Rachid C, Amel A, Naima A (2022) Kinetics and Isotherms modeling of methylene blue adsorption by black carbon using the shells of apricot kernels. Indian J Chem Technol (IJCT) 28(4):412–420
27. Adhami S, Ghorbanpoor H, Berat A, Kapucu S, Nurbas M, Hüseyin A (2018) A novel approach for water treatment by using activated carbon: apricot kernel shell. Eskişehir Osmangazi Üniversitesi Mühendislik ve Mimarlık Fakültesi Dergisi 26(1):1–7
28. Šoštarić TD, Petrović MS, Pastor FT, Lončarević DR, Petrović JT, Milojković JV, Stojanović MD (2018) Study of heavy metals biosorption on native and alkali-treated apricot shells and its application in wastewater treatment. J Mol Liq 259:340–349
29. Ahmadzadeh S, Rezayi M, Karimi-Maleh H, Alias Y (2015) Conductometric measurements of complexation study between 4-Isopropylcalix [4] arene and Cr3+ cation in THF–DMSO binary solvents. Measurement 70:214–224
30. Hashem A, Aniagor C, Taha GM, Fikry M (2021) Utilization of low-cost sugarcane waste for the adsorption of aqueous Pb (II): kinetics and isotherm studies. Curr Res Green Sustain Chem 4:100056
31. Aniagor CO, Elshkankery M, Fletcher AJ, Morsy OM, Abdel-Halim ES, Hashem A (2021) Equilibrium and kinetic modelling of aqueous cadmium ion and activated carbon adsorption system. Water Conserv Sci Eng 6(2):95–104
32. Aniagor C, Abdel-Halim E, Hashem A (2021) Evaluation of the aqueous Fe (II) ion sorption capacity of functionalized microcrystalline cellulose. J Environ Chem Eng 9(4):105703
33. Dubey S, Gusain D, Sharma YC (2016) Kinetic and isotherm parameter determination for the removal of chromium from aqueous solutions by nanoalumina, a nanoadsorbent. J Mol Liq 219:1–8
34. Hashem A, Aniagor C, Hussein D, Farag S (2021) Application of novel butane-1, 4-dioic acid-functionalized cellulosic biosorbent for aqueous cobalt ion sequestration. Cellulose 28(6):3599–3615
35. Hashem A, Aniagor CO, Nasr MF, Abou-Okeil A (2021) Efficacy of treated sodium alginate and activated carbon fibre for Pb (II) adsorption. Int J Biol Macromol 176:201–216
36. Iqbal M, Saeed A, Zafar SI (2009) FTIR spectrophotometry, kinetics and adsorption isotherms modeling, ion exchange, and EDX analysis for understanding the mechanism of Cd2+ and Pb2+ removal by mango peel waste. J Hazard Mater 164(1):161–171
37. Bilba K, Arsene M-A, Ouensanga A (2007) Study of banana and coconut fibers: botanical composition, thermal degradation and textural observations. Bioresour Technol 98(1):58–68
38. Han R, Zhang L, Song C, Zhang M, Zhu H, Zhang L (2010) Characterization of modified wheat straw, kinetic and equilibrium study about copper ion and methylene blue adsorption in batch mode. Carbohydr Polym 79(4):1140–1149
39. Rezayi M, Heng LY, Kassim A, Ahmadzadeh S, Abdollahi Y, Jahangirian H (2012) Immobilization of tris (2 pyridyl)

methylamine in a PVC-membrane sensor and characterization of the membrane properties. Chem Central J 6(1):1–6
40. Das K, Ray D, Bandyopadhyay N, Sengupta S (2010) Study of the properties of microcrystalline cellulose particles from different renewable resources by XRD, FTIR, nanoindentation, TGA and SEM. J Polym Environ 18(3):355–363
41. Nabili A, Fattoum A, Passas R, Elaloui E (2016) Extraction and characterization of cellulose from date palm seeds (Phoenix dactylifera L.). Cellul Chem Technol 50:1015–1023
42. Omorogie MO, Babalola JO, Unuabonah EI, Song W, Gong JR (2016) Efficient chromium abstraction from aqueous solution using a low-cost biosorbent: Nauclea diderrichii seed biomass waste. J Saudi Chem Soc 20(1):49–57
43. Kumari P, Sharma P, Srivastava S, Srivastava M (2006) Biosorption studies on shelled Moringa oleifera Lamarck seed powder: removal and recovery of arsenic from aqueous system. Int J Miner Process 78(3):131–139
44. Sokker H, Abdel-Halim ES, Aly AS, Hashem A (2004) Cellulosic fabric wastes grafted with DMAEMA for the removal of direct dyes. Adsorpt Sci Technol 22(9):679–692
45. Mays T (2007) A new classification of pore sizes. Stud Surf Sci Catal 160:57–62
46. Aniagor CO, Abdulgalil AG, Safri A, Elhmmali M, Hashem A (2022) Preparation of amidoxime modified biomass and subsequent investigation of their lead ion adsorption properties. Clean Chem Eng 2:100013
47. Fiol N, Villaescusa I (2009) Determination of sorbent point zero charge: usefulness in sorption studies. Environ Chem Lett 7(1):79–84
48. Horsfall Jnr M, Spiff AI (2005) Effects of temperature on the sorption of Pb2+ and Cd2+ from aqueous solution by Caladium bicolor (Wild Cocoyam) biomass. Electron J Biotechnol 8(2):43–50
49. Wen X, Du C, Zeng G, Huang D, Zhang J, Yin L, Tan S, Huang L, Chen H, Yu G (2018) A novel biosorbent prepared by immobilized Bacillus licheniformis for lead removal from wastewater. Chemosphere 200:173–179
50. Vaghetti JC, Lima EC, Royer B, Brasil JL, da Cunha BM, Simon NM, Cardoso NF, Noreña CPZ (2008) Application of Brazilian-pine fruit coat as a biosorbent to removal of Cr (VI) from aqueous solution—kinetics and equilibrium study. Biochem Eng J 42(1):67–76
51. Kumar KV, Porkodi K (2007) Mass transfer, kinetics and equilibrium studies for the biosorption of methylene blue using Paspalum notatum. J Hazard Mater 146(1-2):214–226
52. Hashem A, Hammad HA, Al-Anwar A (2016) Modified Camelorum tree particles as a new adsorbent for adsorption of Hg (II) from aqueous solutions: kinetics, thermodynamics and non-linear isotherms. Desalin Water Treat 57(50):23827–23843
53. Hashem A, Ahmad F, Fahad R (2008) Application of some starch hydrogels for the removal of mercury(II) ions from aqueous solutions. Adsorp Sci Technol 8(26):563–579
54. Hashem A, Al-Anwar A, Nagy NM, Hussein DM, Eisa S (2016) Isotherms and kinetic studies on adsorption of Hg (II) ions onto Ziziphus spina-christi L. from aqueous solutions. Green Process Synth 5(2):213–224
55. Aniagor CO, Afifi M, Hashem A (2021) Modelling of basic blue-9 dye sorption onto hydrolyzed polyacrylonitrile grafted starch composite. Carbohydr Polymer Technol Appl 2:100141
56. Langmuir I (1918) The adsorption of gases on plane surfaces of glass, mica and platinum. J Am Chem Soc 40(9):1361–1403
57. Rangabhashiyam S, Nakkeeran E, Anu N, Selvaraju N (2015) Biosorption potential of a novel powder, prepared from Ficus auriculata leaves, for sequestration of hexavalent chromium from aqueous solutions. Res Chem Intermed 41(11):8405–8424
58. Hashem A, Aniagor CO, Badawy SM, Taha GM (2021) Novel application of the esterification product of 2, 3-dihydroxybutanedioic acid and cellulosic biomass for cobalt ion adsorption. Korean J Chem Eng 38(11):2256–2264
59. Hashem A, Fletcher AJ, El-Sakhawy M, Mohamed LA, Farag S (2020) Aminated hydroximoyl camelthorn residues as a novel adsorbent for extracting Hg(II) from contaminated water: Studies of isotherm, kinetics, and mechanism. J Polym Environ 9(28):2498–2510
60. Mohapatra RK, Parhi PK, Pandey S, Bindhani BK, Thatoi H, Panda CR (2019) Active and passive biosorption of Pb (II) using live and dead biomass of marine bacterium Bacillus xiamenensis PbRPSD202: kinetics and isotherm studies. J Environ Manag 247:121–134
61. Bulgariu L, Lupea M, Bulgariu D, Rusu C, Macoveanu M (2013) Equilibrium study of pb (ii) and cd (ii) biosorption from aqueous solution on marine green algae biomass. Environ Eng Manag J (EEMJ) 12(1):183–190
62. Nir S, Undabeytia T, Yaron-Marcovich D, El-Nahhal Y, Polubesova T, Serban C, Rytwo G, Lagaly G, Rubin B (2000) Optimization of adsorption of hydrophobic herbicides on montmorillonite preadsorbed by monovalent organic cations: interaction between phenyl rings. Environ Sci Technol 34(7):1269–1274
63. Razmi FA, Ngadi N, Wong S, Inuwa IM, Opotu LA (2019) Kinetics, thermodynamics, isotherm and regeneration analysis of chitosan modified pandan adsorbent. J Clean Prod 231:98–109
64. Chen S, Qin C, Wang T, Chen F, Li X, Hou H, Zhou M (2019) Study on the adsorption of dyestuffs with different properties by sludge-rice husk biochar: adsorption capacity, isotherm, kinetic, thermodynamics and mechanism. J Mol Liq 285:62–74
65. Abonyi M, Aniagor C, Menkiti M (2019) Effective dephenolation of effluent from petroleum industry using ionic-liquid-induced hybrid adsorbent. Arab J Sci Eng 44(12):10017–10029
66. Muñoz AJ, Espínola F, Moya M, Ruiz E (2015) Biosorption of Pb (II) ions by Klebsiella sp. 3S1 isolated from a wastewater treatment plant: kinetics and mechanisms studies. Biomed Res Int 2015:719060
67. Ho Y-S, McKay G (1999) Pseudo-second order model for sorption processes. Process Biochem 34(5):451–465
68. Namasivayam C, Sangeetha D (2008) Application of coconut coir pith for the removal of sulfate and other anions from water. Desalination 219(1-3):1–13
69. Febrianto J, Kosasih AN, Sunarso J, Ju Y-H, Indraswati N, Ismadji S (2009) Equilibrium and kinetic studies in adsorption of heavy metals using biosorbent: a summary of recent studies. J Hazard Mater 162(2-3):616–645
70. Nazari M, Halladj R (2014) Adsorptive removal of fluoride ions from aqueous solution by using sonochemically synthesized nanomagnesia/alumina adsorbents: an experimental and modeling study. J Taiwan Inst Chem Eng 45(5):2518–2525
71. El Haddad M, Slimani R, Mamouni R, ElAntri S, Lazar S (2013) Removal of two textile dyes from aqueous solutions onto calcined bones. J Assoc Arab Univ Basic Appl Sci 14(1):51–59
72. Sun D, Zhang X, Wu Y, Liu X (2010) Adsorption of anionic dyes from aqueous solution on fly ash. J Hazard Mater 181(1-3):335–342

73. Özcan AS, Erdem B, Özcan A (2004) Adsorption of acid blue 193 from aqueous solutions onto Na–bentonite and DTMA–bentonite. J Colloid Interface Sci 280(1):44–54
74. Can M (2016) Investigation of the factors affecting acid blue 256 adsorption from aqueous solutions onto red pine sawdust: equilibrium, kinetics, process design, and spectroscopic analysis. Desalin Water Treat 57(12):5636–5653
75. Allah MA, Taqui SN, Syed UT, Syed AA (2019) Development of sustainable acid blue 113 dye adsorption system using nutraceutical industrial Tribulus terrestris spent. SN Appl Sci 1(4):1–18
76. Khalid K, Ngah WS, Hanafiah M, Malek NS, Khazaai SN (2015) Acid blue 25 adsorption onto phosphoric acid treated rubber leaf powder. Am J Environ Eng 5(3A):19–25
77. Binaeian E, Tayebi H-A, Shokuhi Rad A, Afrashteh S (2018) Adsorption of acid blue on synthesized polymeric nanocomposites, PPy/MCM-41 and PAni/MCM-41: Isotherm, thermodynamic and kinetic studies. J Macromol Sci A 55(3):269–279
78. Balarak D, Zafariyan M, Igwegbe CA, Onyechi KK, Ighalo JO (2021) Adsorption of acid blue 92 dye from aqueous solutions by single-walled carbon nanotubes: isothermal, kinetic, and thermodynamic studies. Environ Processes 8(2):869–888

Publisher's note Springer Nature remains neutral with regard to jurisdictional claims in published maps and institutional affiliations.